2013

Electron Energy Dependent Charging Effects of Multilayered Dielectric Material

Gregory Wilson
Utah State University

JR Dennison
Utah State Univesity

Amberly Evans Jensen
Utah State University

Justin Dekany

Recommended Citation

Wilson, G., Dennison, J. R., Jensen, A. E., & Dekany, J. (2013). Electron Energy-Dependent Charging Effects of Multilayered Dielectric Materials. IEEE Transactions on Plasma Science, 41(12), 3536–3544. doi:10.1109/TPS.2013.2288356

Electron Energy Dependent Charging Effects of Multilayered Dielectric Materials

Gregory Wilson, JR Dennison, Amberly Evans Jensen and Justin Dekany

***Abstract*— Measurements of the charge distribution in electron-bombarded, thin-film, multilayer dielectric samples showed that charging of multilayered materials evolves with time and is highly dependent on incident energy; this is driven by electron penetration depth, electron emission and material conductivity. Based on the net surface potential's dependence on beam current, electron range, electron emission and conductivity, measurements of the surface potential, displacement current and beam energy allow the charge distribution to be inferred. To take these measurements, a thin-film disordered SiO_2 structure with a conductive middle layer was charged using 200 eV and 5 keV electron beams with regular 15 s pulses at 1 nA/cm^2 to 500 nA/cm^2. Results show that there are two basic charging scenarios which are consistent with simple charging models; these are analyzed using independent determinations of the material's electron range, yields, and conductivity. Large negative net surface potentials led to electrostatic breakdown and large visible arcs, which have been observed to lead to detrimental spacecraft charging effects.**

***Index Terms*—Spacecraft charging, electron emission electron range, conductivity, multilayer materials, dielectrics**

I. Introduction

This research investigates the formation and evolution of internal charge distributions produced in multilayer dielectrics by incident electron fluxes, focusing on materials with thin film surfaces, where thicknesses are comparable to penetration depths of the incident electrons. Thermal and optical coatings, nanoscale and microscale composite materials and electronic devices, and contamination layers all have applications where they fall within these thickness ranges. Further complications arise when different energy beams penetrate through layers of a composite material, depositing charge and energy in different conducting or insulating regions which may or may not be grounded.

As noted by Ferguson [1] and Bodeau [2], from a practical standpoint perhaps the most critical spacecraft systems—in terms of spacecraft charging—are solar arrays and the related high power distribution systems. The solar cells (now often multilayered on a scale of the wavelengths of incident light) and associated coverglasses and optical coatings, are very important examples of the kind of poorly characterized, evolving, inhomogeneous, multilayered materials routinely subject to contamination and surface modification that are addressed by this research.

As spacecraft enter into the space environment, they are constantly subjected to varying levels of charge fluxes, electrons with energies between 200 eV and 100 keV being the principle culprit [3]. Electrons at these energies can penetrate most thin films with thicknesses less than 1 μm. If care is not taken in spacecraft design and material selection, deleterious effects may occur as the deposited charges generate electric fields large enough to cause electrostatic discharge which can often result in damage to materials, components and spacecraft. To mitigate these detrimental effects, understanding of the internal charge evolution within materials used in the construction and shielding of spacecraft is essential.

Currently spacecraft charging codes are largely limited to analysis of bulk materials. Therefore, it is of importance to develop charging models for thin film multilayer dielectrics and contamination layers that can help identify effective strategies for incorporating multilayer/contamination models into charging codes such as NASCAP 2K, SPENVIS, NUMIT and DICTAT.

Ground-based experiments serve a central role in this process, not only to validate the models, but also to characterize proposed spacecraft materials and the charging and discharging processes. Measurements [4] of the internal charge distribution of materials exposed to electron fluxes allow the resulting electric fields to be predicted. However, such direct methods, such as the PEA method, currently only have special resolutions from ~3 μm to ~10 μm, which is thicker than most penetrable surface layers for energies with higher fluxes in space. Inference of the charge distributions is often necessary through indirect measurements [5-9] or modeling [10].

Determination of surface potentials and currents flowing into and out of a material are more readily measured and provide useful evidence to determine internal charge distributions. As shown below, more indirect measurements of electron penetration depth, electron yield and material conductivity are often employed. While the first two properties are highly energy dependent, the material conductivity has only slight dependence on energy (through the radiation induced conductivity (RIC) mechanism), but is highly temperature dependent. Because high insulating materials generally have higher yields and cannot quickly dissipate accumulated charge, they are of particular concern

Research was supported by funding from the NASA James Goddard Space Flight Center and a Utah State University Undergraduate Research and Creative Opportunities grant.

Greg Wilson, JR Dennison, Amberly Evans and Justin Dekany are with the Materials Physics Group in the Physics Department at Utah State University in Logan, UT 84322 USA (e-mail: GregdWilson@gmail.com, JR.Dennison@usu.edu). Evans, Wilson, and Dekany are graduate students in the Physics Department at USU. Dennison is a professor in that department.

Color versions of one or more figures in this paper are available online at http://ieeexplore.ieee.org.

Digital object identifier .

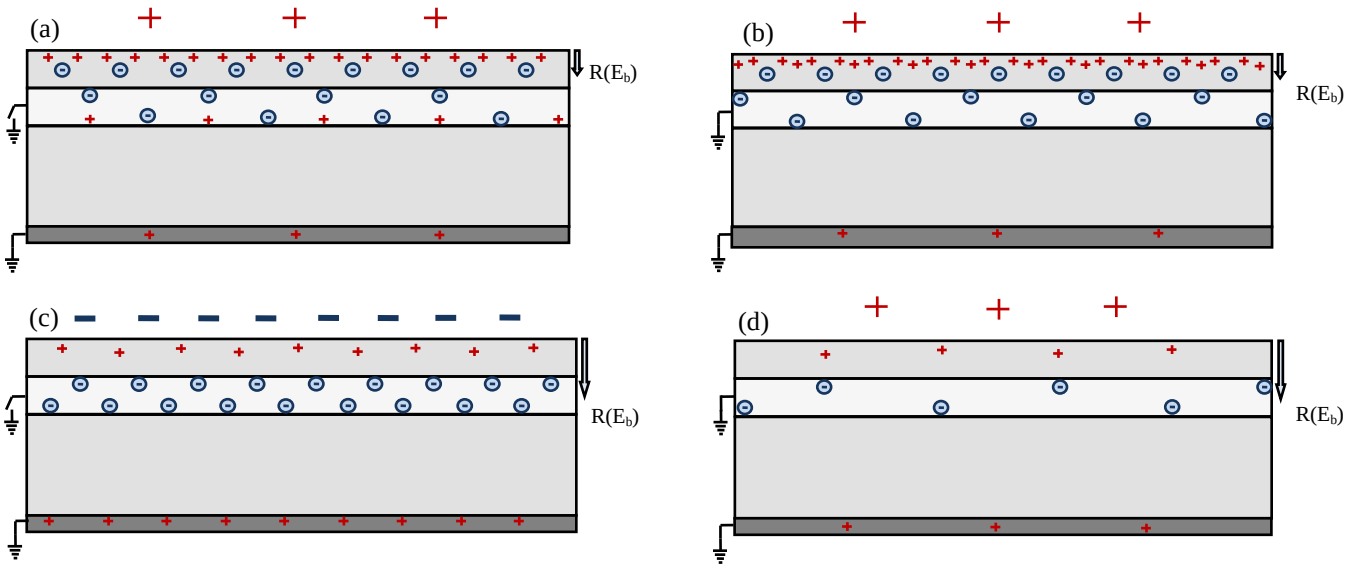

Fig. 1. Charging models for a multilayer dielectric with a conducting middle layer: (a) surface dielectric deposition with low energy electron beam and ungrounded conductive layer, (b) surface dielectric deposition with low energy electron beam and grounded conductive layer (c) conductive layer deposition with high energy electron beam and ungrounded conductive layer (d) conductive layer deposition with high energy electron beam and grounded conductive layer. Electrons are shown as blue circles ⊖ and positive charge centers (holes) as red +. Positive (a,b,d) and negative (c) surface voltages are indicated.

for spacecraft charging. Using these material properties, simple models have been developed which can predict net surface potentials, electrode currents, and the likelihood of electrostatic discharge. While the independent characterization of each of these individual material properties is important [11-14] it is the interplay between these processes that define the time evolution of the charge distribution [15].

We begin with a brief description of instrumentation and experimental design. We present an overview of electron range, electron yield and electron transport, and then describe their interconnectivity with the net surface potential and electrode currents. Finally, measurements for two different energy regimes which define two charging scenarios (charge deposition in the surface dielectric or conductive layer) are interpreted in terms of our multilayer model.

II. Experimentation

In order to investigate the charging of multilayer dielectric materials, pulsed charging experiments were conducted using multilayered dielectric materials of a disordered SiO_2-based optical coating, a conductive middle layer, and an SiO_2 substrate. Tests were made with the conductive layer both grounded and ungrounded. Experiments were conducted in the Utah State University (USU) ultrahigh vacuum electron emission test chamber [16], modified for observations of low intensity UV/VIS/NIR glow over a broad range of sample temperatures [17,18]. A block diagram of the experimental system used is shown in Fig. 1 of [19].

A low energy electron gun [Staib, EK-5-S1] was used, that can deliver a well-characterized, low-flux beam (typically ~50 pA/cm^2 to 1 μA/cm^2) over an energy range of 20 eV to 5 keV. The defocused electron beam produced a nearly Gaussian beam profile at the sample with about ±30% uniformity over a ~3 cm diameter beam spot. Beam fluxes were monitored with a Faraday cup. Beam current densities of 20±1 nA/cm^2 at 200 eV and 2.7±1 nA/cm^2 at 5 keV were used for the experiments reported here, with an exposed sample area of 4.9±0.2 cm^2. The samples were subjected to short duration periods (t_{on}≈15 s) of electron bombardment using a monoenergetic electron beam with beam energies of either 200 eV or 5 keV. This pulsed method allowed us to periodically monitor the surface potential; although current measurements could be made continuously, surface potential measurements require that the incident current was off.

Currents were measured from the back of the mirror to ground and between the conductive layer and ground when the conductive layer was grounded, using fast sensitive picoammeters with <0.2 pA resolution [20]. After each ~15 s pulse, the surface potential was measured using a high impedance non-contact electrostatic voltage probe with a range from ~1 V to ~10 kV and a resolution of ≲0.5 V; details of this instrument are given by Hodges [5,6]. The time between these pulses, t_{off}≈84 s, was limited by the time required to take a surface voltage measurement. Total time for each experimental run was on the order of 1 hr or until equilibrium was reached or electrostatic breakdown was observed. To confirm that near-equilibrium was achieved, a several tests of a few hours duration were conducted.

Samples (2.5 cm diameter) were prepared with thin film (~120 nm thick) disordered SiO_2 (fused silica) deposited on ~220 nm thick highly reflective, optically smooth metal (mostly Ag) layers on a 2.7 mm thick fused quartz substrate. The samples were optically cleaned and underwent a ~12 hr vacuum bakeout at ~390 K and <$1\cdot10^{-3}$ Pa while grounded to eliminate adsorbed water, volatile contaminates, and initial embedded charge. Further details of sample preparation and characterization are provided in [19]. Complimentary cathodoluminescence measurements on similar layered disordered SiO_2 samples are described in [17].

III. Theoretical Model

Four experiments are considered as depicted in Fig. 1. The experiments differ in terms of the incident energy and flux, and as is seen below, produce dramatically different results.

Two experiments (a and b) use low incident energy, two consider high incident energy. Two experiments have an ungrounded conducting layer (a and c) and two have a grounded conducting layer (b and d). To interpret the experiments, we must consider three physical phenomena—the electron range, electron yield and the electron transport (conductivity) of the material—and how they are affected by the experimental conditions.

A. Electron Range

The electron range is the maximum distance an electron of a given incident energy can penetrate through a material at a given incident energy, E_b, as the incident electron undergoes a succession of energy loss collisions and ultimately deposits charge at $R(E_b)$ when all energy is expended (see Fig. 2). Figure 2(a) of [19] shows the results of a composite model for the energy dependence of the range spanning from a few eV to 10^7 eV [11]. It is important to be able to approximate the range in this broad energy regime due to the nature of the space environment where the energies of the space plasma fluxes generally lie between ~10 eV and ~10 MeV [3]. Note that for a dielectric held at potential V, the range is actually a function of the "landing energy" $[E_b+q_eV]$, rather than E_b. (q_e<0 is the charge on an electron.) Also, it is important to note that electrons for a monoenergetic beam are not all deposited at a single depth, but rather measurements [4] and modeling [10] show there is a distribution of penetration depths sharply peaked near $R(E_b)$. For the present purposes, the charge layer approximation is sufficient.

Knowing the range of electrons is especially critical for multilayer materials, where the incident energy will determine where and in what layer charge and energy are deposited. The low (200 eV) and high (5 keV) incident energies were selected for these experiments based on range calculations to deposit charge within the dielectric coating and into the conductive layer, respectively. The transition between these two cases occurs at ≲2.6 keV when the electron penetration depth equals the dielectric coating thickness. These two energies also lead to different charging modes: positive charging occurs between the first and second crossover energies at ~160 eV and ~1.4 to 2.1 keV respectively, while negative charging occurs above and below the crossover energies. Given the uncertainties in the second crossover energy and the distribution of actual charge deposition about the range, it is fair to say that a transition from positive charging with charge deposition in the dielectric layer to negative charging with charge deposition in the conducting layer occurs at ~2 keV.

B. Electron Yield

The total electron yield is defined as the ratio of emitted to incident flux and is highly energy dependent [21]. The incident flux is the total number of electrons entering the material from the environment; the emitted flux is the sum of backscattered and secondary electrons, as shown in Fig. 2. Backscattered electrons undergo a quasi-elastic collision near the surface and backscatter, imparting no net charge to the material. Secondary electrons are generated by incident electrons that undergo collisions near the surface, which impart energy to several other electrons in the material. Some of these other electrons then escape the material's surface leading to net charge loss. When the total yield is less than unity, charging is negative. When the total yield exceeds unity, the material's surface becomes positively charged due to a deficit of electrons. As the net surface potential reaches a potential of a few volts positive, some secondary electrons are re-attracted to the surface which then can recombine with electron holes. This re-attraction effectively creates an upper limit on the net surface potential in the positive net surface potential charging regime.

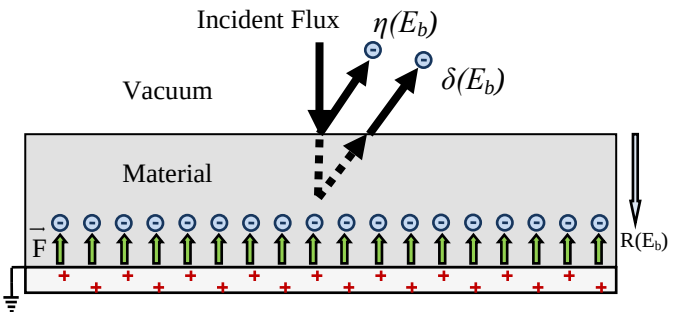

Fig. 2. Diagram of incident electron flux impinging on a generic material. $\eta(E_b)$ denotes the backscattered yield for electrons that originate within the incident beam or that have emission energies E>50 eV. $\delta(E_b)$ denotes the secondary yield for electrons liberated from within the material or that have emission energies E<50 eV. The total yield for all emission energies is the sum of the secondary and backscattered yield; $Y(E_b)= \eta(E_b)+ \delta(E_b)$. $R(E_b)$ is the incident energy-dependant electron penetration depth (range) [9]. Electric fields arise due to charge in the embedded layer(s) and on the grounded planes which can lead to charge transport of the embedded charge layer and displacement currents resulting from charge accumulation and charge migration toward the grounded planes. How easily charge can move depends on the conductivity of the material.

As with the range, the yield is actually a function of the "landing energy" $[E_b+q_eV]$ rather than E_b. Dynamic emission models provide models for yield as a function of surface voltage or charging. A simple model for surface voltage (or time) dependence of the yield for negative charging for $E_b>E_2$, based on a charging capacitor was proposed by Thomson [22]:

$$[1 - Y(t; E_b + q_eV_s)] = [1 - Y(E_b + q_eV_s)]e^{-(Q(t)/\tau_Q)} \quad \text{for } 0 \geq q_eV_s(t) \geq (E_2 - E_b) \qquad (1)$$

τ_Q is a decay constant for the exponential approach of the yield to unity, as charge $Q(t)$ is accumulated with elapsed time and E_2 is the second crossover energy.

C. Conductivity

The conductivity of a material determines how easily a deposited charge layer can move through the material in response to an electric field, $J(t) = \sigma(t)F(t)$; each term can be time-dependant. These electric fields, F, are produced by the embedded charge layers, the depletion layer, and the conductive planes in the material as modeled in Figs. 1 and 2. The measured currents will have two terms, a particle current conductivity proportional to the conductivity and a displacement current due to the change in the electric field due to charge accumulation:

For conditions considered here, we assume the conductivity has only two terms, the equilibrium (dark current) conductivity and radiation induce conductivity; we neglect contributions for polarization, diffusion and dispersion based on arguments related to the time dependence of these contributions compared with our experimental times [23]. For low electron fluxes the conductivity, $\sigma(t)$, is a static

conductivity that approaches the equilibrium (dark current) conductivity of the material, σ_{DC}. For fused silica the equilibrium conductivity at room temperature is $\sigma_{DC}\approx1.5\cdot10^{-19}$ $(\Omega\text{-cm})^{-1}$ [24]; temperature-dependant conductivity of fused silica is shown in Fig. 2(d) of [19]. Because σ_{DC} of fused silica is so low, charge movement over the duration of our tests can be neglected and we can assume perfect insulators as a first order approximation for our models.

For high fluxes, however, Radiation Induced Conductivity (RIC) must be taken into account in regions where the incident beam penetrates. RIC is the enhanced conductivity that results from the energy deposited in this volume. It is a function of the dose rate, $\dot{D}$, which is the power deposited by incident radiation per unit mass [25]. RIC is expressed in terms of the dose rate as a power law with ½<Δ<1 [25]:

$$\sigma_{RIC}(\dot{D}) = k_{RIC}\dot{D}^{\Delta} \tag{2}$$

The dose rate in a homogeneous material is approximately inversely proportional to the volume in which radiation energy is deposited; this volume is approximately equal to the beam cross sectional area times R [26]: therefore,

$$D(\dot{E}_b) \equiv {\partial D}/{\partial t} = \frac{E_b\, J_b}{\rho_m\, R(E_b)\, q_e} \tag{3}$$

where J_b is the incident beam current density and ρ_m is the mass density. The dose rates, $\dot{D}(E_b)$, for disordered SiO_2 and Ag are shown in Fig. 3(a) of [19]. Figure 3(b) of [19] shows $\sigma_{RIC}(E_b)$ for SiO_2. Both $\dot{D}$ and σ_{RIC} exhibit incident energy-dependent maxima as a consequence of the minimum in the range expression seen in Fig. 2(a) of [19]. For fused silica $\Delta\approx1$ and $k_{RIC}\approx1.7\cdot10^{-16}$ $(\Omega\text{-cm-rad/s})^{-1}$ at room temperature [24]. For the low and high energy tests, σ_{RIC} is approximately $1\cdot10^{-10}$ $(\Omega\text{-cm})^{-1}$ at J_b=20 nA/cm^2 and $1\cdot10^{-12}$ $(\Omega\text{-cm})^{-1}$ at J_b=2 nA/cm^2, respectively. Because these values are relatively high, the charge bodies will reach equilibrium in the RIC region on smaller time scales than we can detect. To calculate the deposited power for each layer we can multiply (3) by the amount of material radiated and, for subsequent layers, replace E_b with the energy at which the electrons enter that particular layer. Figure 3 shows the deposited power for our multilayered samples as a function of incident energy, calculated in this manner

D. Surface Potential

Using these three physical phenomena, we can now build a model to relate the internal charge distribution to the net surface potential. Once an insulator with a grounded backplane is exposed to an electron flux, to first order, the surface potential charges according to a simple capacitance model [5,23]

$$V_S(t) = V_{inj}(t)\left(1 - e^{-t\sigma(t)/\varepsilon_0\varepsilon_r}\right) \tag{4}$$

where ε_0 is permittivity of free space, ε_r is the relative permittivity of the material, and V_0, the long term equilibrium potential, is

$$V_0 = \frac{\bar{J}_b}{\sigma_o}[D - R(E_b)] \tag{5}$$

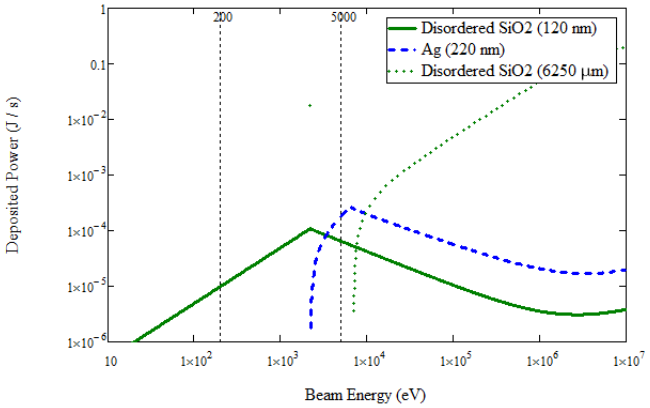

Fig. 3. Estimated deposited power for our multilayered system with a flux density of 10 nA/cm^2 and a beam area of 4.9 cm^2 as a function of incident energy. Refer to [9] for explanation of calculation methods.

where $\bar{\bar{J}}_b = J_b\left[t_{on}/(t_{on}+t_{off})\right]$ is the incident beam current density corrected for the duty cycle. For the experiments here, $\left[{\sigma(t)}/{\varepsilon_0\varepsilon_r}\right] \ll t$, thus the exponential term in (4) can be neglected. To account for the charge-dependant electron emission given by (1), we write the injection voltage as [23]

$$V_{inj}(t) = V_o(t)[1 - Y(E_b)]\left(1 - e^{-Q(t)/\tau_Q}\right) \tag{6}$$

An additional effect to account for is the re-attraction of secondary electrons to the charged surface [27]. For negative surface potentials at which Y<1, these emitted electrons will receive a "boost" in energy of $|q_eV_s|$ as they leave the surface; the number of emitted electrons is largely unaffected by negative surface potentials. As the material charges more and more negatively, the deposited charge layer can produce an electric field which exceeds the limits of the material, leading to electrostatic breakdown. This breakdown voltage may or may not be reached, depending on the conductivity of the material and the current density of the electron beam. If the charge dissipation to ground can keep pace with the amount of charge deposited, then the material will reach an equilibrium voltage lower than the breakdown voltage. When breakdown does occur, conduction paths may be formed which then decrease the materials ability to hold charge. This will lead to a negative net surface potential less than the original net surface potential before breakdown. For fused silica at room temperature, the dielectric breakdown strength is ~$3.5\cdot10^7$ V/m and the relative permittivity for fused silica is 3.5 [24].

For positive surface potentials at which Y>1, more electrons are ejected from near the surface than penetrate into the material. A depletion charge layer forms that is more positive than the deeper negative charge layer deposited by the electron beam. As the net surface potential becomes more positive, the emitted secondary electrons become re-attracted to the surface, where they can recombine with depletion sites (holes). By convention secondary electrons have <50 eV emission energy; emission spectra for essentially all uncharged materials are peaked at ~2 eV to 5 eV and the vast majority of emitted secondary electrons have energies <10 eV. Since secondary electron emission spectra are peaked at low energies, even small positive surface potentials re-attract large

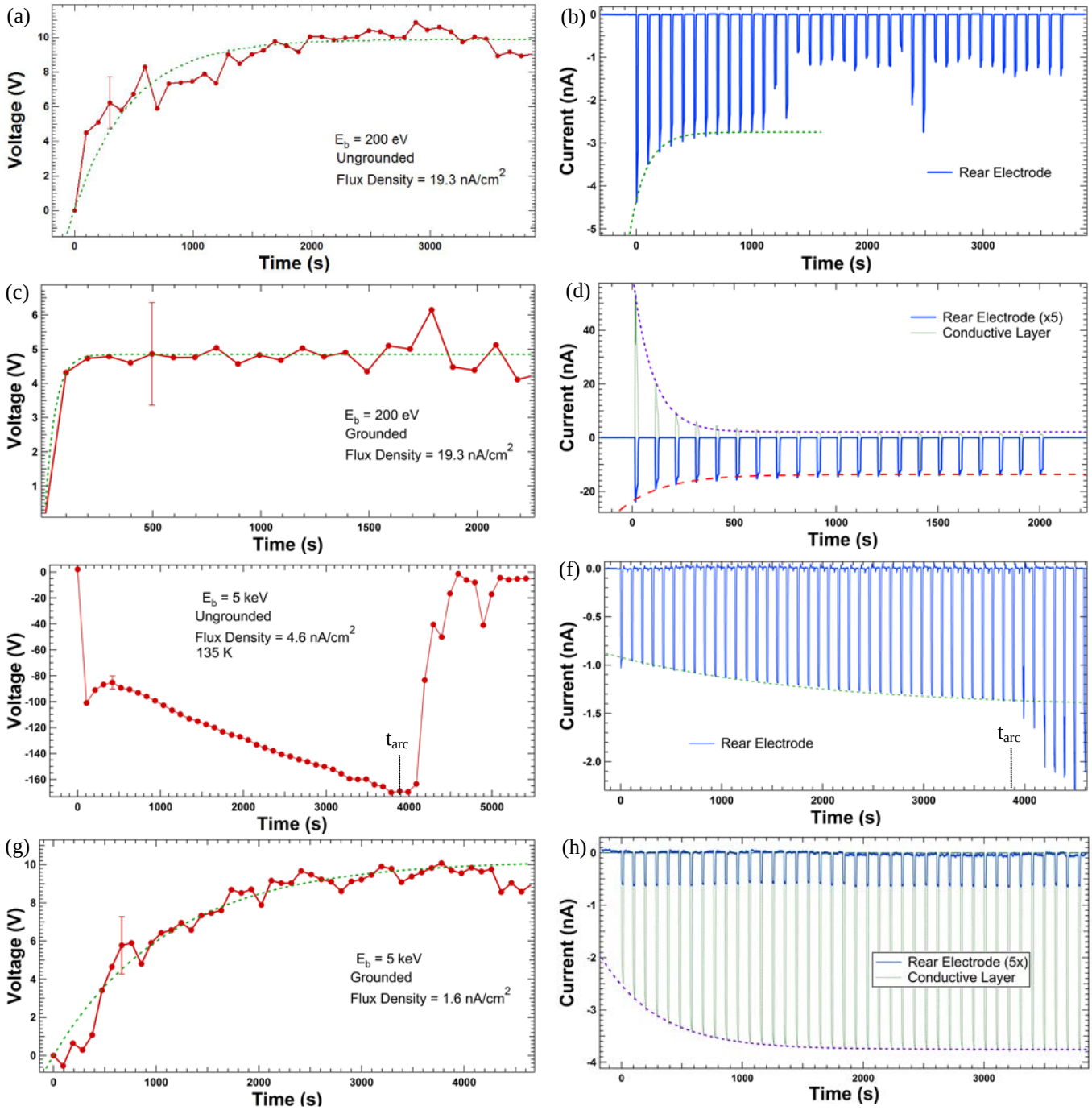

Fig. 4. Measurements of surface potentials vs time (a, c, e, g) and rear electrode and conductive layer currents vs time (b, d, f, h) for: (a, b) surface dielectric deposition with low energy electron beam and ungrounded conductive layer; (c, d) surface dielectric deposition with low energy electron beam and grounded conductive layer; (e, f) conductive layer deposition with high energy electron beam and ungrounded conductive layer; and (g, h) conductive layer deposition with high energy electron beam and grounded conductive layer. (a,b,c,d,g,h) were measured at 298 K and (e,f) at 135 K. Exponential fits for the voltage was based on Eq. 6 with (a) τ=475 s (τ_Q =6.6 μC), (c) τ=45 s (τ_Q =0.63 μC), (g) τ=1137 s (τ_Q =1.33 μC). Exponential fits for currents were based on Eq. 8 with (b) τ=139 s (τ_Q =1.93 μC), (d) conductive layer τ=99 s (τ_Q =1.37 μC), rear electrode τ=206 s (τ_Q =2.86 μC) (f) τ=2880 s (τ_Q =3.37 μC), (h) τ=462 (τ_Q =0.54 μC).

numbers of secondary electrons; this means that positive potentials are self-limiting and seldom exceed ~10 V [12].

The charging scenarios described above are often described by a double dynamic layer model (DDLM) [28-30]. The DDLM model has been used to describe static measurement of surface voltage [5] and electron yields [21]. [31] discusses the dependence of satellite charging in terms of threshold charging due to re-attraction and changes in the yield.

E. Electrode Current

The current measured at the grounded rear electrode includes two contributions, the free charge transport current density, J_c, and the charge displacement current density, J_{disp}.

$$J_{elec}(t) = J_{elec}^{c}(t) + J_{elec}^{displacement} = \sigma(t)F(t) + \epsilon_o\epsilon_r \frac{\partial F(t)}{\partial t} \quad (7)$$

For the time-independent conductivity estimated above and for general voltage expressions for the parallel plate geometry, it can be shown that this current is given by [23]

$$J(t) = \bar{J}_b(t)[1 - Y(E_b)]\left(1 - e^{-Q(t)/\tau_Q}\right)\left\{1 + \left[1 + {}^{\tau_d}/_{t_{on}}\right]^{-1}\right\} \quad (8)$$

IV. Results

The surface voltage and rear electrode and conducting layer current data presented in Fig. 4 correspond to the four scenarios identified in Section III; (A) surface dielectric deposition (with 200 eV electron beam) with ungrounded conductive layer; (B) surface dielectric deposition (with 200 eV electron beam) with grounded conductive layer; (C) conductive layer deposition (with 5 keV electron beam) with grounded conductive layer; and (D) conductive layer deposition (with 5 keV electron beam) with ungrounded conductive layer. Results and fits for each of the four scenarios are given in the four sections below, along with discussions of their similarities and differences and interpretation of results in terms of the model of Section III.

A. Surface Dielectric Deposition—Ungrounded

For a 200 eV monoenergetic electron beam the electron range in disordered SiO_2 is approximately 3 nm [19]. At this depth, the electrons just penetrate into the first layer, but do not reach the conductive layer. The total yield for disordered SiO_2 at this energy is ~1.3>1[19,32], which leads to a positive charge depletion layer. Thus, we should see a self-limiting positive net surface potential due to a net deficit of electrons; this agrees with the sign of the measured net surface potential as shown in Fig. 4(a). Voltage equilibrium is reached after ~2000 s at V_o=9.9±0.5 V, which is only ~4% of the beam voltage and is consistent with re-attraction of most secondary electrons to the positively charged surface. V_s and J_{elec} (see (6) and (8), respectively) are both reduced by ~96% from incident current (J_b) values, which is the product of a duty cycle factor [t_{on} / (t_{on} + t_{off})] = 15% and a yield factor [1-Y(200eV)] ≈ 30%. The magnitude of the equilibrium voltage predicted by this reduction factor is ~80% of the measure V_0. The magnitude of the displacement current predicted by this reduction factor is ~60% of the measured displacement current amplitude of ~1.58 nA in Fig. 4(b).

The surface voltage data in Fig. 4(a) is fit well by an exponential decay from (6), with decay time constant τ=475±50 s or in terms of *incident charge*, τ_{QI}=6.6 μC. Comparison with the yield data dependant on *deposited charge* (see Fig. 2(c) of [19]) with a charge constant τ_{QD}=56 fC suggests that only 15 ppb of the incident charge is absorbed. Because the conductive layer is ungrounded, a charge separation in the metal will occur due to the electric field produced in the top layer, but it will have negligible effect on the net surface potential.

Figure 4(b) shows the rear electrode current as a function of time. The "comb" structure of the current data clearly reflects the current duty cycling with t_{on}=15 s and t_{off}=84 s. The mean values of the rear electrode current in each current spike shows a long term saturation as expressed as an exponential decay (solid curve in Fig. 4(b)) as modeled by a simplified version of (8) with J_{sat}= $\bar{J}_b(t)[1 - Y(E_b)]$; the displacement term is neglected due to the long time scales between surface voltage measurements. Fused silica has very low dark current conductivity of ~$3\cdot10^{-19}$ (ohm-cm)$^{-1}$ [24] with a corresponding decay time of ~$1\cdot10^6$ s; so charge movement from the layer deposited at $R(E_b)$ to the conducting layer is negligible on the 10^3 s time scale of our measurements, but our fits require an extra additive offset constant, J_{offset}. Thus we must have a significant charge dissipation mechanism active such as polarization, RIC, an arc-induced leakage path, or surface leakage currents. Results show that our saturation current is J_{sat}=1.58 nA, with offset, J_{offset}=-4.34 nA giving current equilibrium J_{eq}= J_{sat}+ J_{offset} =-2.76 nA and decay time constant τ_D=139±12 s or in terms of incident charge, τ_Q=1.9 μC. The significant variations evident in the rear electrode current (Fig. 4(b)) after ~1200 s suggest that sustained small-scale arcing begins in the ungrounded conducting layer.

Closer examination of the rear electrode current for a single ~15 s pulse clearly shows this displacement current along with a saturation current. Thus, an exponential fit to the current decay for a single pulse is the summation of the exponential of the short term saturation current plus the exponential of the displacement current as modeled in Fig. 5(a). For surface dielectric deposition, the exponential displacement has a time constant of 4.1±0.1 s (0.38±0.09 μC) while the saturation time constant is 1±1 s (0.1±0.1 μC) which is much longer than the time constant for RIC conduction; τ_{RIC}=6 ms based on (2), the beam parameters, and a measured RIC value [24]. Thus, we speculate that charge motion during the beam on times is driven, at least largely, by something besides RIC or that the literature value for RIC is inaccurate for the specific type of disordered SiO_2 used in our experiments; low temperature RIC experiments are currently in progress [33].

B. Surface Dielectric Deposition—Grounded

For a 200 eV electron beam with a grounded conductive layer, we expect similar behavior for the surface voltage as seen for the ungrounded scenario.

Positive surface voltage is observed in Fig. 4(c), as expected. Voltage equilibrium is reached after ~400 s at V_o=4.8±0.4 V, fit well by an exponential decay from (6), with decay time constant τ=45±14 s (0.6±0.2 μC). It is speculated that the decay time constant is an order of magnitude smaller than the ungrounded case due to the image charge plane formed in the grounded conducting layer.

Because electrons are free to move from ground to the conductive plane, we should see a positive current on the electrometer into the conductive layer to form this image plane. This is seen in the conductive layer current in Fig. 4(d). Note that the initial current for the uncharged sample is ~52 nA, is also approximately half of the estimated incident current for an incident current density of ~19 nA/cm^2 and a sample collection area of 4.9 cm^2. The current falls off exponentially with a long-term saturation time constant of 99±4 s (1.37±0.05 μC) while the rear electrode current for the grounded case has long term saturation time constant τ=206±30 s (2.9±0.4 μC). These fitting parameters are within ~30% of those found for the ungrounded case. This long term saturation current is driven by the equal magnitude mirror charge layer on the metal layer at a distance only ~240 nm closer to the rear electrode than for the ungrounded case.

C. Conductive Layer Deposition—Grounded

For a 5 keV monoenergetic electron beam the electron range in disordered SiO_2 is ~560 nm [19]. The electrons penetrate through the surface dielectric and well into the conductive layer (see Fig. 3). The incident current was reduced to ~1.6 nA/cm^2 for the high energy beam. The total yield for disordered SiO_2 at this energy is <1 (~0.7 from [19] and ~0.4 from [32]), which should lead to a negative net surface potential in Fig. 4(g). However, because the conductive layer is grounded, charge will dissipate quickly from the conductive layer. Although the electron yield is <1 for a 5 keV electron beam, there will still be a positively charged deficit layer near the surface which will behave similar to the low energy scenarios; thus, we should observe a self-limiting small positive potential similar to Fig. 4(a). This is confirmed in Fig. 4(g), where voltage equilibrium is reached after ~2000 s at V_o=9.3±0.4 V. The surface voltage data in Fig. 4(g) is fit well by an exponential decay from (6), with decay time constant τ=1137±93 s (1.3 ± 0.1 μC), which agrees with the fitting parameters in Fig. 4(a) to within 80±%.

Figure 4(h) shows constant, negative and nearly zero rear electrode current; this is expected since the conductive layer is held at ground and excess charge is bled off. This current on the conductive layer can be modeled as an exponential decay (solid curve in Fig. 4(h)), based on (8), with saturation current J_{sat}=1.22 nA, equilibrium current J_{eq}=*-3.76* and decay time constant τ=462 ± 11 s (0.54 ± 0.01 μC).

D. Conductive Layer Deposition—Ungrounded

For a 5 keV electron beam with an ungrounded conductive layer, we expect significantly different behavior than seen for the surface voltage with a grounded conductive layer. The high energy incident electrons deposit negative charge in the conductive layer. Because the conductive layer is ungrounded there will be no fast charge dissipation mechanism. Because there is no limiting behavior from re-attraction of secondary electrons, we should see a high net negative potential. Because of the low conductivity, the charge cannot dissipate through the dielectric substrate to the grounded rear electrode faster than charge is being deposited by the beam, thus the potential will become more and more negative until the produced electric fields exceed the limits of the material or produce fields strong enough to produce arcing from the exposed surface of the conductive layer to the surrounding grounded sample holder which is ~1 mm away.

The initial current (Fig. 4(f)) and voltage behavior (Fig. 4(e)) are indeed markedly different, rising very rapidly to negative voltages beyond -100 V with the first pulse, followed by a short duration reversal for the next three beam pulses. Similar retrograde charging behavior has been reported for FEP, LDPE, and other polymers [34-36]; this has been attributed to (i) trapping/recombination on an increasing trapped charge in regions where RIC becomes active over a finite time and space charge accumulation [34-37] or (ii) defect generation due to beam aging above 100 kGy [38] (our pulses generate only ~5 kGy, so this may not be pertinent for this early affect). Inspecting the separate pulses of Fig. 4(f) we see that there is an obvious displacement current for the first beam pulse as shown in Fig. 5(a), with exponential displacement time constant 0.507 ± 0.008 s (4.0 ± 0.06 nC) and saturation time constant 1.444 ± 0.007 s (11.3 ± 0.06 μC).

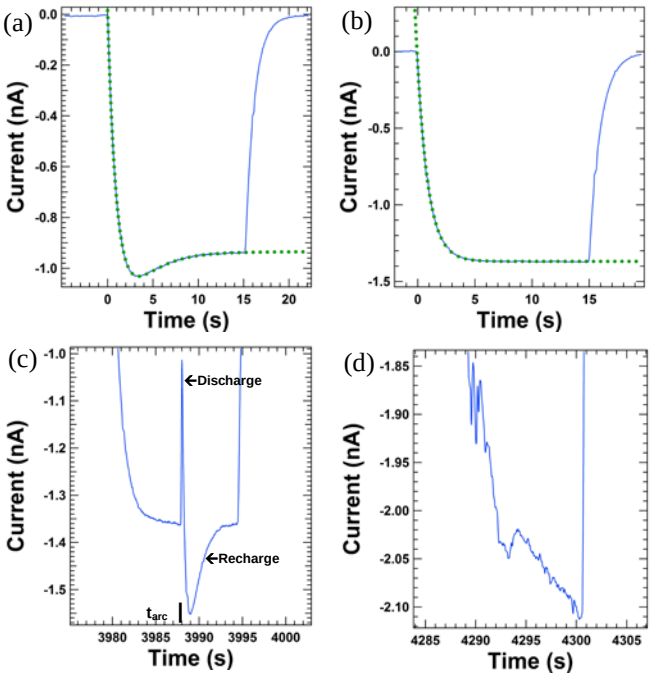

Fig.5. Expanded views of the rear electrode current in Fig. 4(f) for conductive layer deposition with high energy (5 keV) electron beam and an ungrounded conductive layer that is undergoing negative charging. A similar profile is seen in both low energy (200 eV) surface substrate deposition cases in Figs. 4(b) and 4(d). (a) First current pulse with fit based on (8). (b) Current pulse immediately before the first observed arc with fit based on (8). (c) Current during first arc, at t_{arc}=3987 s. (d) Current after subsequent arcing.

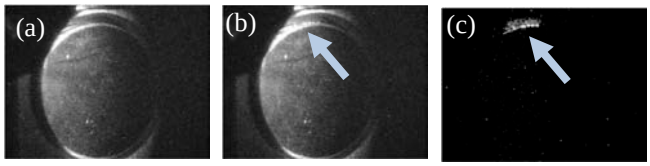

Fig. 6. Visible images of sample with the CCD video camera: (a) immediately before the arc, (b) during the arc, and (c) the first image subtracted from arc image to show the light attributed to the arc. Arrow indicates location of visible arc signature.

This current profile shows similarities to surface voltage measurements for keV beams using pulses of ~1% the fluence of our 15 s pulses [32]. After the fourth beam pulse the displacement current vanishes as shown in Fig. 5(b), with saturation time constant 0.966 ± 0.001 s (7.53 ± 0.007 nC).

After the fourth pulse, the surface voltage again shows a linear increase, but now at a charging rate of ~2.4 V/pulse (very close to the charging rate for full beam current absorption near the bottom of the conductive layer, but ~40 times less than the initial rate during the first pulse). The linear charging at the lower rate continues until the sample reaches -170 V, at which point electric field across the ~1 mm film-to-sample holder gap (with a reasonable field enhancement of ~25 due the aspect ratio and surface roughness [37]) exceeding the breakdown field strength 4 MV/m measured for a ~60 nm thin film of disordered SiO_2 [39,40]. At t_{arc}≈3987 s an electrostatic discharge occurred from the conductive layer to the sample holder, as observed in the imaging instruments (see Fig. 6) and the electrometer (see Fig. 5(c)). In the six subsequent pulses after t_{arc}, the rear electrode current continued to increase to ~50% above the incident beam current (see Fig. 4(f)) as the surface voltage rapidly decreased to near zero potential (see Fig. 4(g)).

Increasing numbers of arcs became apparent in the pulses after t_{arc}, to the point at which currents were quite erratic (see Fig. 5(d)). This is consistent with excess charge leaking from increasing areas of the thin film as successive regions of the thin film experience breakdown, as seen in the discharge study [39,40].

V. Conclusion

Through observation of the net surface potential and the currents from the rear electrode and the conducting plane (when grounded), we were able create a model to infer the internal charge distribution in multilayered samples. Two incident energies were studied, 200 eV and 5 keV, which were chosen as representative of charge deposition within the dielectric coating with positive charging and into the conductive layer with negative charging, respectively. The results showed that the four scenarios of ungrounded dielectric surface deposition, grounded dielectric surface deposition, ungrounded conductive layer deposition and grounded conductive layer deposition led to two net surface potential charging regimes, small positive charging and high negative charging. (The identification of these two charging regimes is consistent with similar studies of charging and electron yields for bulk SiO_2 layers over similar incident energy ranges [32].)

This allowed prediction of electric fields and the likelihood of electrostatic breakdown (which was observed in several runs) in the multilayer material. We found that low energy electrons which embedded themselves in surface layers with yields greater than 1 exhibit a self limiting positive surface potential, which should generally yield a safe spacecraft environment. If these electrons, however, are able to penetrate through one or more surface layers and interact with deeper layers, high negative charging can occur when the material cannot bleed off charge faster than it is injected. With this scenario, the high negative net potentials that can be achieved, can lead to electrostatic discharge and other detrimental charging effects. While the net surface potential showed the charge equilibrium reached after a given pulse, the electrode current data provided additional information about the time evolution of the charges as they reached equilibrium and insight into charge transport and dissipation, displacement currents, charging of internal floating conductors, and precursors to arcing.

Clearly the combination of high resolution surface voltage and electrode current measurements coupled with an accurate model of the evolving charge distribution provide valuable tools to understand both laboratory tests and actual spacecraft charging and arcing events. This builds a framework whereby the charge movement, the net surface potential and the general charge deposition of any thin film multilayer dielectric material can be predicted with reasonable results to help determine the possibility and probability of detrimental spacecraft events such as high negative charging and electrostatic discharge.

ACKNOWLEDGEMENT

We gratefully acknowledge contributions to instrumentation and experimental efforts from Josh Hodges, Robert Johnson, Tamara Jeppsen and Doug Ball of the Materials Physics Group, Michael Taylor for the use of infrared and CCD video cameras, aid with theoretical models from Alec Sim, and useful discussions with Robert Meloy and Charles Bowers of NASA Goddard Space Flight Center.

References

[1] D. C. Ferguson, New Frontiers in Spacecraft Charging," *IEEE Trans. on Plasma Sci.*, **40**(2), 2012, pp.139-143.

[2] Michael Bodeau, "Current and Voltage Thresholds for Sustained Arcs in Power Systems", *IEEE Trans. on Plasma Sci.*, **40**(2), 2012, pp.192-200.

[3] D. Hastings, H. Garrett, Spacecraft-Environment Interactions, New York, NY: Cambridge Press, 1996.

[4] B. Beecken, B. Walling, "Modeling of Deep-dielectric Spacecraft Charging in Realistic Environments with NUMIT2" AIAA 2011-3975, *Proc. 49th AIAA Meeting on Aerospace Sci*., Orlando, FL, 2011.

[5] J.L. Hodges, "*In Situ* Measurements of Electron Beam Induced Surface Voltage of Highly Resistive Materials," MS Thesis, Utah State Univ., Logan, UT, 2012.

[6] J. L. Hodges, A.M. Sim, J. Dekany, G. Wilson, A. Evans, and J.R. Dennison "*In Situ* Surface Voltage Measurements of Layered Dielectrics," *Proc.* 12*th Spacecraft Charging Techn. Conf.*, (Kitakyushu, Japan, May, 2012).

[7] A.R. Frederickson and J.R. Dennison, "Measurement of Conductivity and Charge Storage in Insulators Related to Spacecraft Charging," *IEEE Trans. Nuclear Sci.*, Vol. 50, No. 6, 2003, pp. 2284-2291.

[8] L. Levy, D. Sarrail, and J.M. Siguier, "Conductivity and secondary electron emission properties of dielectrics as required by NASCAP," *3rd European Symp. on Spacecraft Materials in Space Environment*, 1993, pp. 113-123.

[9] R. Coelho, L. Levy, and D. Sarrail, "Charge decay measurements and injection in insulators," *J. App. Phys.*, Vol. 22, No. 9, Sept. 1989, pp. 1406-1409.

[10] W. Kim, "NUMIT 2.0: The official release of the JPL's internal charging code," *Proc.* 12*th Spacecraft Charging Techn. Conf.*, (Kitakyushu, Japan, May, 2012).

[11] G. Wilson and J.R. Dennison, "Approximation of Range in Materials as a Function of Incident Electron Energy," *IEEE Trans. on Plasma Sci.*, **40**(2), 305-310 (2012).

[12] R.C. Hoffmann and J.R. Dennison, "Methods to Determine Total Electron-Induced Electron Yields Over Broad Range of Conductive and Nonconductive Materials," *IEEE Trans. Plasma Sci.*, **40**(2), 2012, pp. 298-304.

[13] J. Dekany, A.M. Sim, J. Brunson, and J.R. Dennison, "Electron Transport Models and Precision Measurements in a Constant Voltage Chamber," *Proc.* 12*th Spacecraft Charging Techn. Conf.*, (Kitakyushu, Japan, May, 2012).

[14] C. Sim, A.M. Sim, J.R. Dennison and M. Stromo, "Defect-Driven Dynamic Model of Electrostatic Discharge and Endurance Time Measurements of Polymeric Spacecraft Materials," *Proc.* 12*th Spacecraft Charging Techno. Conf.*, (Kitakyushu, Japan, May, 2012).

[15] J.R. Dennison, "The Dynamic Interplay Between Spacecraft Charging, Space Environment Interactions and Evolving Materials," *Proc.* 12*th Spacecraft Charging Techn. Conf.*, (Kitakyushu, Japan, May, 2012).

[16] W.Y. Chang, J.R. Dennison, N. Nickles and R.E. Davies, "Utah State University Ground-based Test Facility for Study of Electronic Properties of Spacecraft Materials," *Proc. 6th Spacecraft Charging Techn. Conf.*, (AFRL Sci. Center, Hanscom Air Force Base, MA, 2000).

[17] A. Evans, G. Wilson, J. Dekany, A.M. Sim and J.R. Dennison "Low Temperature Cathodoluminescence of Space Observatory Materials," *Proc.* 12*th Spacecraft Charging Techn. Conf.*, (Kitakyushu, Japan, May, 2012).

[18] J. Dekany, R.H. Johnson, G. Wilson, A. Evans and J.R. Dennison, "Ultrahigh Vacuum Cryostat System for Extended Low Temperature Space Environment Testing," *Proc.* 12*th Spacecraft Charging Techn. Conf.*, (Kitakyushu, Japan, May, 2012).

[19] G. Wilson, J.R. Dennison, A. Evans and J. Dekany, "Electron Energy Dependent Charging Effects of Multilayered Dielectric Materials" *Proc.* 12*th Spacecraft Charging Techn. Conf.*, (Kitakyushu, Japan, May, 2012).

[20] C.D. Thomson, V. Zavyalov, and J.R. Dennison, "Instrumentation for Studies of Electron Emission and Charging from Insulators," *Proc. 8th Spacecraft Charging Techn. Conf.* (NASA Marshall Space Flight Center, Huntsville, Al, October 2003), 15 pp.

[21] R. Hoffmann, "Electron-Induced Electron Yields of Uncharged Insulating Materials," M.S. Thesis, Utah State Univ., Logan, UT, 2010.
[22] C.D. Thomson, "Measurements of the Secondary Electron Emission Properties of Insulators," Ph.D. Dissertation, Utah State Un., Logan, UT, 2004.
[23] J.R. Dennison and A.M. Sim, "Unified Density of States Based Model of Electron Transport and Emission of Spacecraft Materials," *Proc.* 12th *Spacecraft Charging Techn. Conf.*, (Kitakyushu, Japan, May, 2012).
[24] V.E Culler and H.E. Rexford, "Gamma-radiation-induced conductivity in glasses," *Proc. IEEE*, 112(7), pp. 1462, 1965.
[25] J.R. Dennison, J. Gillespie, J.L. Hodges, R.C. Hoffmann, .J. Abbott, A.W. Hunt and R. Spalding, "Radiation Induced Conductivity of Highly-Insulating Spacecraft Materials," in *Application of Accelerators in Research and Industry*, Am. Institut. Phys. Conf. Proc. Series, Vol. 1099, ed. F.D. McDaniel and B. L. Doyle, (Am. Institut. of Phys., Melveille, NY, 2009), pp. 203-208.
[26] J.A. Roth, R. Hoffmann, and J.R. Dennison, 2009, "Effects of Radiation Induced Conductivity on Electrostatic Discharge in Insulating Materials," *Proc. 1st AIAA Atmospheric and Space Environments Conf.* (San Antonio, TX).
[27] N. Nickles, R.E. Davies and J.R. Dennison, "Applications of Secondary Electron Energy- and Angular-Distributions to Spacecraft Charging," *Proc. 6th Spacecraft Charging Techn. Conf.*, (AFRL Sci. Center, Hanscom Air Force Base, MA, Oct. 2000).
[28] J. Cazaux, "Scenario for Time Evolution of Insulator Charging under Various Focused Electron Irradiations," *J. Appl. Phys.* **95**, , 2003, p. 731.
[29] A. Melchinger and S. Hofmann, "Dynamic Double Layer Model: Description of Time Dependent Charging Phenomena in Insulators under Electron Beam Irradiation," *J. Appl. Phys.* **78**, 1995, p. 6224.
[30] X.D. Meyza, Goeuriot, C. Guerret-Piecourt, D. Treheux, and H. Fitting, "Secondary Electron Emission and Self-Consistent Charge Transport and Storage in Bulk Insulators: Application to Alumina," *J. Appl. Phys.* **94**, 2003, p. 5384.
[31] J.R. Dennison, R.C. Hoffmann, and J. Abbott, "Triggering Threshold Spacecraft Charging with Changes in Electron Emission from Materials," Paper AIAA-2007-1098, *Proc. 45th Am. Inst. of Aeronautics and Astronomics Meeting on Aerospace Sci.*, Reno, NV, Jan., 2007.
[32] R. Gallet, J.-P. Goose and Y. Arnal, "Charging experiments on SiO_2 samples under electron irradiation," *Proc. 2001 IEEE 7th Intern. Conf. Solid Dielectrics*, 2001, pp.256-259.
[33] J.R. Dennison and G. Wilson, "Comparison of Radiation Induced Conductivities at Low Temperature," *Am. Phys. Soc. Four Corner Section Meeting*, Socorro, NM, October, 2012.
[34] P. Molinié, P. Dessante, R. Hanna, T. Paulmier, B. Dirassen, M. Belhaj, D.Payan and N. Balcon, "Polyimide and FEP Charging Behavior under Multienergetic Electron-Beam Irradiation", *IEEE Trans. Diel. Elec. Insulation*, **19**(4), 2012, pp. 1215-1220.
[35] P. Molinié, "A Review of Mechanisms and Models Accounting for Surface Potential Decay," *IEEE Trans. on Plasma Sci.*, **40**(2), 167-176 (2012).
[36] R. Hanna, T. Paulmier, P. Molinié, M. Belhaj, D. Bernad, D. Payan, and N. Balcon, Radiation induced conductivity in Teflon FEP irradiated with multi-energetic electron beam," *Proc.* 12th *Spacecraft Charging Techn. Conf.*, (Kitakyushu, Japan, May, 2012).
[37] B. Gross, R.M. Faria, G.L. Leal Ferreira, "Radiation-induced conductivity in Teflon irradiated by x-rays", *J. Appl. Phys.*, Vol. 52, 1981, pp. 571-577.
[38] S. A. Khatipov, "Radiation-Induced Electron Transport Processes in Polymeric Dielectrics (A Review)", *High Energy Chem.*, Vol. 35, No. 5, 2001, pp. 291–307.
[39] A. Anders, *Cathodic Arcs*, Springer Series on Atomic, Optical and Plasma Physics, Vol 50, New York, Springer: 2008.
[40] A. Andersen, C. Sim and J.R. Dennison, "Electrostatic Discharge Properties of Fused Silica Coatings," *Am. Phys. Soc. Four Corner Section Meeting*, Socorro, NM, October, 2012.

Greg Wilson is currently a graduate student at Utah State University (USU) in Logan, UT pursing an MS in physics. He received BS degrees in physics and mathematics from USU in 2011. He has worked with the Materials Physics Group for two years on electron emission and luminescence studies related to spacecraft charging. He also developed a composite model for electron range over a wide range of incident energies applicable to diverse materials.

JR Dennison received the B.S. degree in physics from Appalachian State University, Boone, NC, in 1980, and the M.S. and Ph.D. degrees in physics from Virginia Tech, Blacksburg, VA in 1983 and 1985, respectively. He was a Research Associate with the University of Missouri—Columbia before moving to USU, Logan, UT in 1988. He is currently a Professor of physics at USU, where he leads the Materials Physics Group. He has worked in the area of electron scattering for his entire career and has focused on the electron emission and resistivity of materials related to spacecraft charging for the last two decades.

Amberly Evans is currently a graduate student at USU in Logan, UT pursing an MS in physics. She received BS degrees in physics and chemistry from USU in 2012. She has worked with the Materials Physics Group for five years on electron emission, luminescence and resistivity studies and on MISSE retrieval and post-flight analysis of *SUSpECS*. Much of her work has focused on optical scattering of spacecraft materials.

Justin Dekany is currently a graduate student at USU in Logan, UT pursing an MS in physics. He received a BS degree in physics from USU in 2010. He has worked with the Materials Physics Group for four years on electron transport measurements, electrostatic discharge tests, electron emission measurements, and luminescence studies related to spacecraft charging. He has been the Lab Manager for the Materials Physics Group for the last two years.